Journal of Applied Physics

Thermosize voltage induced in a ballistic graphene nanoribbon junction

Cite as: J. Appl. Phys. **126**, 104302 (2019); https://doi.org/10.1063/1.5111504
Submitted: 27 May 2019 . Accepted: 19 August 2019 . Published Online: 11 September 2019

Alhun Aydin, Jonas Fransson, and Altug Sisman

COLLECTIONS

This paper was selected as an Editor's Pick

View Online Export Citation CrossMark

ARTICLES YOU MAY BE INTERESTED IN

A first-principles study on transport properties of polyacene in zigzag graphene nanoribbon: Configuration, length and doping effects
Journal of Applied Physics **126**, 104501 (2019); https://doi.org/10.1063/1.5118939

Transport properties of topologically non-trivial bismuth tellurobromides Bi_nTeBr
Journal of Applied Physics **126**, 105105 (2019); https://doi.org/10.1063/1.5116369

Dielectric nanoantennas to manipulate solid-state light emission
Journal of Applied Physics **126**, 094104 (2019); https://doi.org/10.1063/1.5108641

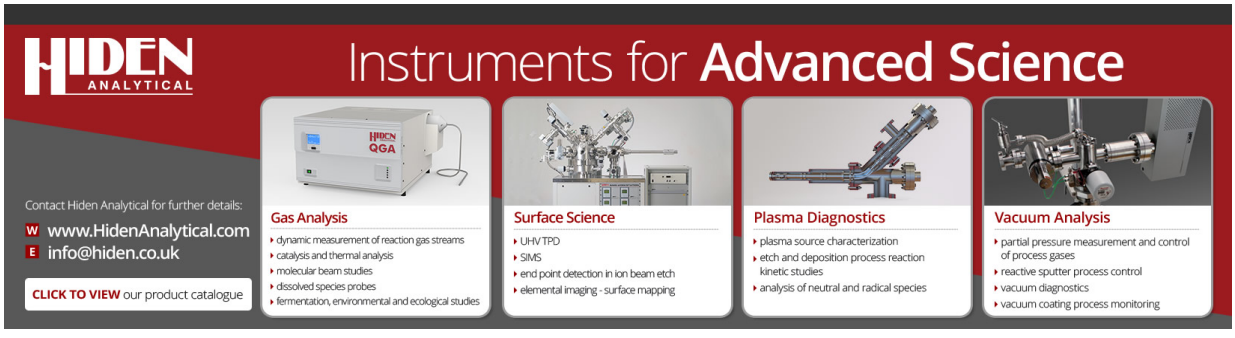

© 2019 Author(s).

Journal of Applied Physics ARTICLE scitation.org/journal/jap

Thermosize voltage induced in a ballistic graphene nanoribbon junction

Cite as: J. Appl. Phys. **126**, 104302 (2019); doi: 10.1063/1.5111504
Submitted: 27 May 2019 · Accepted: 19 August 2019 ·
Published Online: 11 September 2019

View Online Export Citation CrossMark

Alhun Aydin,[1,2] Jonas Fransson,[1] and Altug Sisman[1,2,a)]

AFFILIATIONS

[1]Department of Physics and Astronomy, Uppsala University, Box 516, 75120 Uppsala, Sweden
[2]Nano Energy Research Group, Energy Institute, Istanbul Technical University, 34469 Istanbul, Turkey

[a)]**Electronic mail:** altug.sisman@physics.uu.se

ABSTRACT

A thermoelectric voltage is induced in a junction, constituted of two dissimilar materials under a temperature gradient. Similarly, a thermosize voltage is expected to be induced in a junction made by the same material but having different sizes, so-called thermosize junction. This is a consequence of dissimilarity in Seebeck coefficients due to differences in classical and/or quantum size effects in the same materials with different sizes. The studies on thermosize effects in the literature are mainly based on semiclassical models under relaxation time approximation or even simpler local equilibrium ones where only very general ideas and results have been discussed without considering quantum transport approaches and specific materials. To make more realistic predictions for a possible experimental verification, here we consider ballistic thermosize junctions made by narrow and wide ($n-w$) pristine graphene nanoribbons with perfect armchair edges and calculate the electronic contribution to the thermosize voltage, at room temperature, by using the Landauer formalism. The results show that the maximum thermosize voltage can be achieved for semiconducting nanoribbons and it is about an order of magnitude larger than that of metallic nanoribbons. In the semiconducting case, the thermosize voltage forms a characteristic plateau for a finite range of gating conditions. We demonstrate, through numerical calculations, that the induced thermosize voltage per temperature difference can be in the scale of mV/K, which is high enough for experimental measurements. Owing to their high and persistent thermosize voltage values, graphene nanoribbons are expected to be good candidates for device applications of thermosize effects.

© 2019 Author(s). All article content, except where otherwise noted, is licensed under a Creative Commons Attribution (CC BY) license (http://creativecommons.org/licenses/by/4.0/). https://doi.org/10.1063/1.5111504

I. INTRODUCTION

Thermoelectric effect provides a unique mechanism for direct conversion between heat and electricity. Pioneering works by Hicks and Dresselhaus in 1993[1,2] stimulated extensive research on enhancing thermoelectric efficiency by making use of quantum confined structures.[3] Since then, thermoelectric junctions have been explored in various contexts, such as quantum dots,[4] molecules,[5–7] nanowires,[8] superlattices,[9,10] and graphene.[11–24] Rather than making a junction between electrodes with different materials, a junction between electrodes with the same material but having different sizes may also generate an electrochemical potential difference when a temperature gradient is applied. This potential difference emerges from distinctive classical and/or quantum size effects on the Seebeck coefficients, so-called thermosize effect.[25] The thermosize effect does not only open new optimization possibilities in thermoelectric junctions, but also serves as a new computational and experimental platform for the examination of quantum size effects in different materials. Various studies have been conducted for thermosize effect and their possible applications during the last 15 years.[26–40]

Thermosize effect is initially proposed and designed for junctions between the electrodes of the same material, in which one electrode is at nanoscale but the other one is at macroscale. In this way, the setup constitutes a nano-macro thermosize junction (TSJ).[25] By considering nano-macro as well as nano-micro junctions, thermodynamic performance analyses of cycles working with both classical and quantum thermosize effects have been examined thoroughly.[26–39] On the other hand, these studies in the literature are based on either semiclassical models using relaxation time approach or even simpler local thermodynamic equilibrium ones. Therefore, some general ideas and results have been discussed without considering quantum transport approaches and specific materials. In addition, despite the fact

that quantum size effects are expected to be much more prominent for ballistic transport,[41] the thermosize effect in the quantum ballistic regime has been completely overlooked.

In this study, we demonstrate, through numerical calculations, that the induced thermosize voltage between quantum ballistic electrodes can become high enough to experimentally verify and use for device applications. Here, we choose armchair graphene nanoribbons (AGNRs), having both width and length smaller than the phase coherence length, as well as the characteristic mean free path of electrons, as electrode material in our TSJ. We calculate the transmission function of the graphene nanoribbons (GNRs), described using a tight-binding model, in the transmission (Landauer) formalism. From the transmission, we obtain the thermoelectric transport coefficients and thermosize potential for GNR TSJs as a function of size, aspect ratio, and temperature. We examine, using a few viable examples, the thermoelectric properties of GNRs as well as thermosize voltage in GNR TSJs.

GNR is a perfectly suitable material for the TSJ due to its ballistic transport properties at room temperature.[42–44] Moreover, owing to the strong size dependence of the electronic properties and corresponding band structure,[14,24,45–47] GNRs serve as one of the best materials to investigate size-dependent properties. They may, in addition, be good candidates for realizations of TSJs, considering the efforts on their practical usage.[18,23,44] Depending on the shape of their edges, GNRs are classified as zig-zag or armchair GNRs. Since the thermoelectric performance of armchair GNRs is shown to be better than that for zig-zag GNRs in general,[13] we consider narrow-wide (n–w) armchair GNR TSJs in this study.

II. THERMOSIZE JUNCTION OF GRAPHENE NANORIBBONS AND ITS MODELING

A schematic view of the setup we propose is presented in Fig. 1, showing a TSJ of a narrow and wide (n–w) armchair GNRs. A temperature gradient, defined between by a set of hot thermal reservoir ($T_H = 310$ K) at the left end and a cold thermal reservoir ($T_C = 300$ K) at the right. At the cold end of the junction, the two GNRs are interconnected to one another, both electrically and thermally. An insulating layer separating the GNRs from each other extends into the hot reservoir, thereby electrically separating the GNRs along the transport direction. Under zero external bias voltage, an electrochemical potential difference is induced between the hot and cold reservoirs across the GNRs, emerging as a response

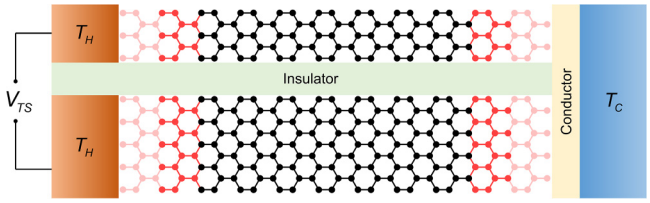

FIG. 1. A schematic (not to scale) of a thermosize junction (TSJ) of narrow-wide (n–w) graphene nanoribbons (GNRs) with armchair edges (armchair GNR). Temperature difference ($T_H > T_C$) at the ends of the same material with different sizes gives rise to thermosize voltage V_{TS}.

to the applied temperature difference. However, because of the unequal sizes (widths) of the two GNRs, the induced electrochemical potential differences across the GNRs are different. Hence, since the electrochemical potentials of the GNRs are equal at the cold side, a voltage difference is generated between the GNRs at the hot end of the junction. This phenomenon is referred to as the thermosize effect. Note that both transport and transverse directions are much smaller than the mean free path and comparable with the de Broglie wavelength of electrons. The width per dimer is around 0.12 nm and depending on the number of dimers, the width of GNRs ranges from 0.6 nm (5 GNRs) to 3 nm (25 GNRs).

In order to quantify our discussion, we construct a mathematical model corresponding to the system in Fig. 1. The GNRs can be effectively described by a tight-binding Hamiltonian,

$$\mathscr{H} = -t \sum_{\langle i,j \rangle} c_i^\dagger c_j + H.c., \tag{1}$$

where the sum runs over all nearest-neighbors $\langle i, j \rangle$, t is the hopping rate, the operator $c_i^\dagger$ (c_i) creates (annihilates) an electron on the ith site. The on-site energy is chosen to be zero relative to the Fermi energy which we set to $\epsilon_F = 0$. For the quantum transport calculations, we have employed the software KWANT,[48] which allows for the construction of the tight-binding model and calculation of total transmission function $\mathscr{T}(\varepsilon)$. The nearest-neighbor hopping rate $t = 2.7$ eV, which successfully describes the electronic properties of GNRs in the absence of lattice deformation.[42,49,50] Thanks to the weak electron-phonon coupling in GNRs, even at room temperature, phonon scattering of electrons is negligible.[12,14,42] We assume that the electrical contacts are perfectly transmitting, which leads to that the thermoelectric coefficients only depend on the widths of GNRs. In this way, we can focus on solely the influence of the size (width) difference.

Depending on its width, the GNR can be either semiconducting or metallic.[45] The width of the GNR is associated with the number N of dimer lines across its width, and we shall use this number to label the N-armchair GNR. The junctions constructed at the interface between semiconducting and metallic GNRs cannot be considered as TSJs, since semiconducting and metallic GNRs are actually different types of materials in this context. Therefore, such a setup constitute a usual thermoelectric junction, and while size also matters for such junctions, we shall omit this possibility since we want to focus on thermosize effects only. Before we approach the construction of TSJs, we first investigate the thermoelectric transport properties like conductance, Seebeck coefficient, and power factor of GNRs as a function of the width, in order to understand their individual thermoelectric properties at room temperature for different widths of AGNRs.

By employing transmission formalism,[51] the dimensionless transport integral in the linear response regime reads

$$I_\alpha = \int [\beta(\varepsilon - \mu)]^\alpha \beta f(\varepsilon)[1 - f(\varepsilon)]\mathscr{T}(\varepsilon)d\varepsilon, \tag{2}$$

where $\beta = 1/(k_B T)$, k_B is the Boltzmann constant, T is the temperature, α indicates the energy moment index, μ denotes the chemical potential, and $f(\varepsilon) = 1/\{\exp[\beta(\varepsilon - \mu)] + 1\}$ is the Fermi-Dirac

© Author(s) 2019

distribution function. In terms of the transport integral I_α, the electrical conductance and Seebeck coefficient are then written as

$$G = \frac{2e^2}{h} I_0, \tag{3a}$$

$$S = -\frac{k_B}{e}\frac{I_1}{I_0}, \tag{3b}$$

where e is the electron charge, h is the Planck constant, and the factor 2 signifies spin degeneracy. The power factor P is then given by $P = GS^2$.

In Figs. 2(a) and 2(b), we plot the transmission coefficients as a function of the chemical potential μ for a few GNRs with different N ranging between 5 and 17. From these plots, it can be concluded that we can classify the GNRs into two groups with distinct conducting properties. The first class, comprising the 5-, 11-, 17-armchair GNRs, as well as the 23-armchair GNR (not shown here), all have zero bandgap, and would, therefore, be considered as metallic. The second class, containing the 9-, 13-, 15-armchair GNRs, complemented by the 7-, 19-, 21-, and 25-armchair GNRs (not given here), have finite bandgaps and are, thereby, here regarded as semiconducting. This latter class is identified by bandgaps in the order of more than 400 meV (25-armchair GNR giving the minimum bandgap), which, hence, provides viable semiconducting properties at room temperature. Our results are in very good agreement with the previous ones in the literature.[44]

From the transmission coefficient, we extract the Seebeck coefficient and power factor. In Fig. 2(c), we plot the modulus of the Seebeck coefficients and in Fig. 2(d) the power factor (both normalized to their corresponding maximum values) as a function of the electrochemical potential μ, for three metallic and three semiconducting GNRs. Since we want to focus only on a certain type of carriers in the TSJs, we consider conduction electrons for which $\mu > 0$ (n-type). As expected,[14,17] the Seebeck coefficients of the semiconducting GNRs are substantially more than two orders of magnitude, larger than that for the corresponding metallic ones. This is understood to be an effect of the finite bandgap around the Dirac point for the semiconducting GNRs. In spite of the huge difference between the maximums of Seebeck coefficients of semiconducting and metallic GNRs, the discrepancy between their corresponding power factors is not comparably large. Naturally, this originates from the (much) larger conductances of the metallic GNRs compared to those of semiconducting ones in the pertinent ranges of chemical potentials. Thus, from the result presented in Fig. 2, it can be concluded that the thermosize voltage should be significant for semiconducting GNRs at low chemical potentials.

III. THERMOSIZE VOLTAGE IN GRAPHENE NANORIBBON JUNCTIONS

In a TSJ under zero external bias voltage, the applied temperature difference first serves as the sole driving force for the charge current. Then, because of the zero steady-state current condition, an electrochemical potential difference builds up as an opposite driving force for the current. The net particle current inside each GNR of the TSJ can be expressed as

$$I_{\text{net}} = I_H - I_C = \frac{2e}{h}\int [f(\mu_H, T_H) - f(\mu_C, T_C)]\mathscr{T}(\varepsilon)d\varepsilon, \tag{4}$$

under the assumption that $\mathscr{T}(\varepsilon)$ is the same for left and right moving particles. Here, the hot (cold) end of the junction is denoted by H (C). The emergent thermosize voltage between the narrow and wide GNRs is then defined as

$$V_{TS}(\mu_C, T_H, T_C) = \left(\mu_H^n\big|_{I_{net}=0} - \mu_H^w\big|_{I_{net}=0}\right)/e. \tag{5}$$

In Fig. 3, we plot the thermosize voltages for three different (a) semiconducting and (b) metallic GNR TSJ configurations, as a

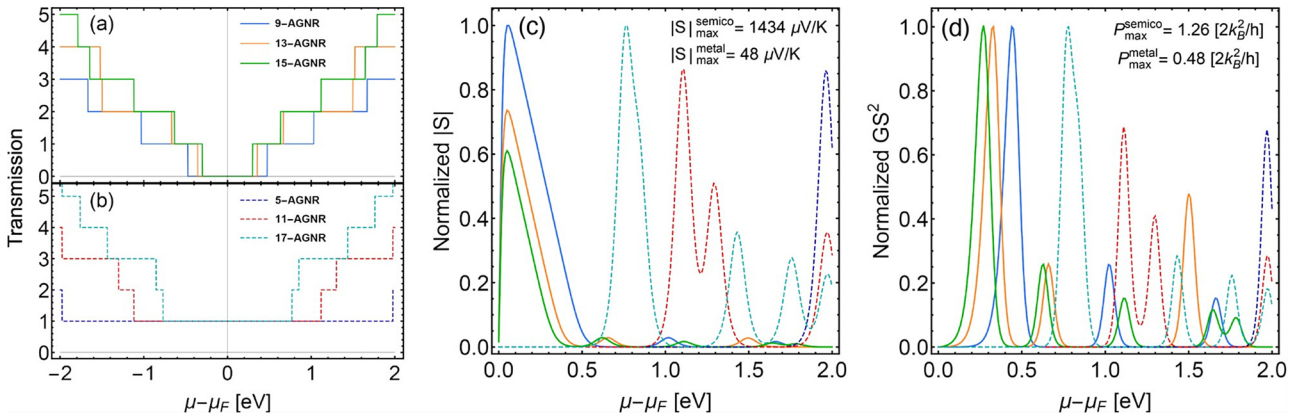

FIG. 2. The transmission coefficient $\mathscr{T}$ for (a) semiconducting and (b) metallic GNRs, (c) Seebeck coefficient, and (d) power factor (the last two are normalized to their maximum values) at 300 K as a function of the chemical potential for GNRs having 6 different widths, where the 9-, 13-, and 15-armchair GNRs exhibit semiconducting, while the 5-, 11-, and 17-armchair GNRs show metallic transport properties.

© Author(s) 2019

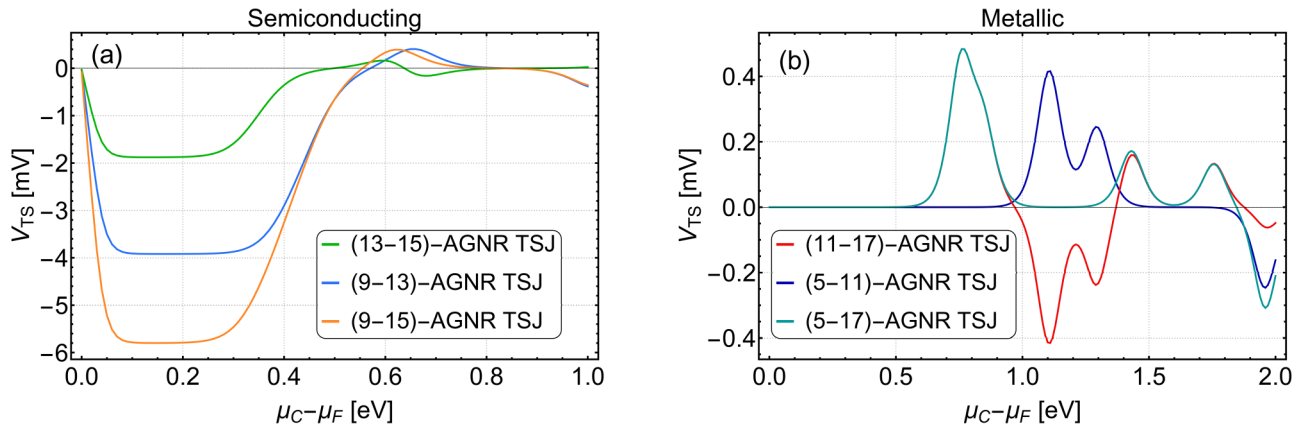

FIG. 3. Thermosize voltage changes with the chemical potential of the cold side for (a) semiconducting and (b) metallic TSJs of armchair GNRs for various ($n-w$) width combinations for 10 K temperature difference at room temperature.

function of the chemical potential μ_C of the cold side. For semiconducting TSJs, the magnitude of thermosize voltage grows rapidly with increasing values of μ_C in the vicinity of zero and then forms an extended plateau for a wide range of μ_C and returns back to a negligible voltage in an oscillatory fashion for large values of μ_C. The thermosize voltage in the metallic TSJs, on the other hand, remains vanishingly small for a wide range of μ_C and becomes finite only at large values of μ_C, acquiring an oscillatory behavior about zero voltage for increasing μ_C. The results, hence, suggest that for large values of electrochemical potential μ_C, the thermosize voltages generated by semiconducting TSJs, on the one hand, and metallic TSJs, on the other, are comparable in magnitude. By contrast, for small values of μ_C, the thermosize voltages generated in semiconducting TSJs are about 10 times larger than that in the corresponding metallic TSJs. Comparing the results in Figs. 2(b) and 3(a), we see that thermosize voltage is sizable in the same range of chemical potentials where the Seebeck coefficient peaks. The large magnitude of the thermosize voltage and the characteristic plateau for semiconducting TSJs suggest that this setup should be promising for the experimental demonstration of the effect.

It can also be noticed that the thermosize voltages in metallic TSJs are similar in magnitude for different GNR configurations. This can be contrasted by the observation that the thermosize voltages for different GNR configurations in semiconducting TSJs differ by almost a factor of three. In fact, the results in Fig. 3(a) indicate that a simultaneous increase of the widths of both n and w GNRs tends to decrease the thermosize voltage. This is an expected behavior since the quantum size effects become decreasingly important for larger sizes. Higher values of the aspect ratio between the widths of n and w GNRs, however, cause higher thermosize voltage. This behavior clearly suggests that the larger the difference in magnitudes of quantum size effects, the larger thermosize voltage can be obtained. In both semiconducting and metallic cases, the sign of the thermosize voltage can be controlled by the chemical potential.

The aspect ratio of $n-w$ is important for the design of the TSJ. Since the semiconducting TSJs give much higher thermosize voltages, we restrict our further considerations to this class of junctions. The plots in Fig. 4 show the variations of the thermosize voltage as a function of the aspect ratio, for different values of μ_C. In Fig. 4(a), we vary the aspect ratio n/w, between $7/25 \lesssim 0.3$ and $21/25 \gtrsim 0.8$, of the junction by keeping the width of the wide GNR constant. Here, we consider only the configurations of GNRs, which leads to semiconducting TSJs. The results clearly show that the larger the thermosize voltage becomes, the smaller the aspect ratio is, and it decreases monotonically with increasing aspect ratio. However, since quantum size effects become more prominent for the smaller sizes, we also checked whether a near unity aspect ratio can still sustain a considerable thermosize voltage. In Fig. 4(b), we plot the thermosize voltage as a function of aspect ratio in the range between $7/9 \gtrsim 0.77$ and $19/21 \lesssim 0.91$ by keeping the difference $N_w - N_n$ between the wide and narrow GNRs constant. These results clearly show that even an aspect ratio near unity may not be detrimental for small enough GNRs constituting the junction. Intrinsic quantum size effects may very well become stronger and make the potential difference high enough even though the widths of GNRs are close to each other. This perspective is also corroborated by the fact that the thermosize voltage monotonically decreases with increasing widths of the GNRs, keeping the difference $N_w - N_n$ fixed. For wider GNRs, the intrinsic quantum size effects become increasingly similar in the two GNRs, which, therefore, tends to diminish the electrochemical potential difference between the electrodes.

In Fig. 5, we investigate how the variations in temperatures influence the induced voltage of a thermosize junction for various cold side chemical potential values. As an example, we choose 9–15 AGNR TSJs with semiconducting behavior, since it gives the highest thermosize voltage values. In Fig. 5(a), we plot the thermosize voltages with respect to the temperature difference at both ends by keeping the hot side temperature fixed at $T_H = 400$ K. By controlling the doping concentration or gate voltage, the cold side chemical potential can be kept constant while the temperature of the cold side changes. Within the examined range of temperature values, the thermosize voltage increases in general by increasing the temperature difference, or in other words, decreasing the cold side temperature.

© Author(s) 2019

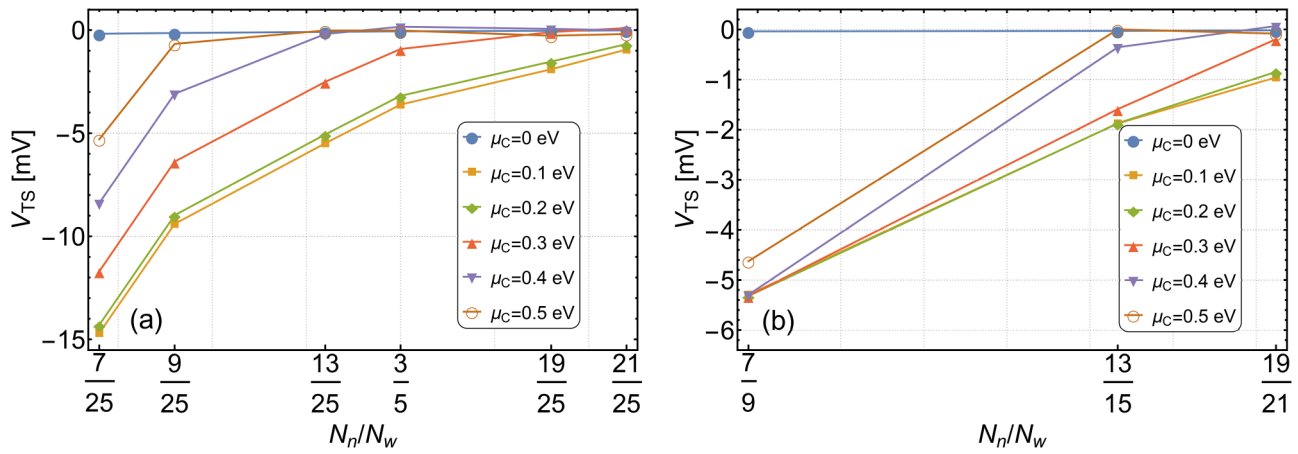

FIG. 4. Aspect ratio dependences of thermosize voltage in semiconducting TSJs plotted for different chemical potential values (a) by changing the narrow side while keeping the wide side constant and (b) by changing both sides while keeping $N_w - N_n = 2$.

This is actually a consequence of an expected linear dependency of induced voltage on temperature difference. Conversely, for $\mu_C = 0.1\,\text{eV}$, there is an optimal temperature difference which maximizes the thermosize voltage. Therefore, increasing the temperature difference further does not increase the thermosize voltage indefinitely. This is because increasing the temperature difference at constant chemical potential causes a shift to higher chemical potentials ($\mu_C - \mu_F$) in the characteristic curves of the thermosize voltage given in Fig. 3(a) at a constant temperature difference. Although for $\Delta T = 10\,\text{K}$, $\mu_C = 0.1\,\text{eV}$ corresponds to the plateau, for $\Delta T = 100\,\text{K}$, it corresponds to the region where a sharp change occurs on the left part of the plateau, which has lower voltage values than that of the plateau. In fact, this behavior is not unique to that particular value of chemical potential, but increasing the temperature difference will result in a similar behavior for other μ_C values as well. However, since we restrict the course of this article into high temperatures, we will not decrease the temperature any lower than the room temperature.

In Fig. 5(b), thermosize voltage changes with the cold side temperature by fixing the temperature difference at $\Delta T = 10\,\text{K}$. Thermosize voltage slowly decreases with increasing temperature, because this is a quantum effect and quantum size effects become weaker when de Broglie wavelengths of particles are smaller with increasing temperature. As expected, $\mu_C = 0.1$ and $\mu_C = 0.2$ give the highest thermosize voltage values, since they correspond to the persistent thermosize voltage plateau shown in Fig. 3(a). The effect of decrement in Fig. 5(b) diminishes when the cold side chemical potential gets lower or higher than the values corresponding to the

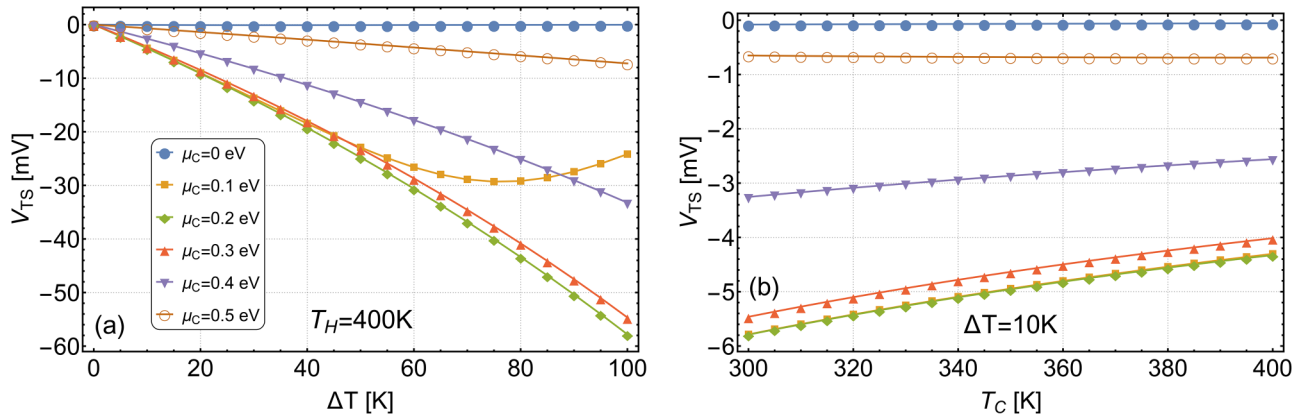

FIG. 5. Thermosize voltage of 9–15 semiconducting AGNR TSJs changes (a) with temperature difference at a constant hot side temperature, $T_H = 400\,\text{K}$, (b) with a cold side temperature by keeping the temperature difference constant at $\Delta T = 10\,\text{K}$. Six different cold side chemical potential values are considered. The legend in subfigure (a) also applies to subfigure (b).

© Author(s) 2019

voltage plateau. This is due to the fact that quantum size effects (and so thermosize effects) are less present for the chemical potentials that do not correspond to the voltage plateau. When we compare both figures, one can see that the effect of temperature difference is much higher than by just changing the temperature at a constant temperature difference.

IV. DISCUSSION AND CONCLUSION

In conclusion, we predict that thermosize effect can experimentally be verified and examined by constructing GNR TSJs. In the studied setups, we predicted voltages per unit temperature difference in the order of mV/K, at room temperature. For a comparison, conventional thermoelectric voltage induced in a wide p-n graphene junction can reach up to 0.2 mV/K,[20,23] which is on the same order of the thermosize voltage. GNRs provide better thermoelectric performance than graphene because of its further reduced dimensionality, which causes enhancement due to size effects. Thermoelectric voltage in p-n armchair GNR junctions can reach up to 5 mV/K.[13,17] Note that thermosize voltage values are always lower than the half of the maximum thermoelectric voltage that can be obtained in the same type of p-n GNR junctions. This is because the Seebeck coefficients of p-type and n-type GNRs are almost symmetric with respect to Fermi level and thermoelectric voltage can take advantage of the full magnitude of it, which is always larger than twice of the thermosize voltage. However, by taking advantage of the size difference as well, it can be possible to go beyond the existing thermoelectric junctions by combining the quantum size effects. Large Seebeck coefficient suggests a large thermosize voltage. On the other hand, the thermal conductivity of perfect GNRs is also very high. To tackle this, there have been some thoughts to control the thermal conductivity of nanomaterials, including introducing structural defects,[52] constructing superlattices,[53] or branched structures.[54] Effects of impurity/defects on thermosize voltage are under consideration as an extension of this study.

The formation of the induced electrochemical potential gradient in response to the applied temperature difference will take some finite amount of time and will be affected by the boundary scatterings between GNRs and the insulator. For this particular study, we neglect this boundary scattering since the thermosize voltage is defined under zero net current, which is relevant after the electrochemical potential gradient is formed. In our fully ballistic study, electrons reach from one terminal to the other without any boundary scattering.

The suitability of GNRs for TSJs is accompanied by their preserved ballistic transport properties and low electron-phonon coupling at room temperature, as well as the strong quantum size dependence of their electronic properties and band structures. In this realm, the atomically thin GNR allows us to explore the thermosize effect upon approaching the quantum limit. One shall notice that our results may be regarded as an upper limit for the thermosize voltage, since deviations from these ideal results may arise from, for example, impurities, contact resistances, and incoherences. We nonetheless believe that the effect remains sufficiently large in GNRs due to state-of-the-art capabilities to manufacture ultraclean graphene.[55,56] In a realistic device, the GNR most likely has to be deposited on a substrate, which may open up new opportunities in the design of energy conversion devices based on quantum size effects.

ACKNOWLEDGMENTS

Authors are very grateful to Uppsala University for its open access support.

REFERENCES

[1]L. D. Hicks and M. S. Dresselhaus, "Effect of quantum-well structures on the thermoelectric figure of merit," Phys. Rev. B **47**, 12727 (1993).
[2]L. D. Hicks and M. S. Dresselhaus, "Thermoelectric figure of merit of a one-dimensional conductor," Phys. Rev. B **47**, 16631 (1993).
[3]P. Pichanusakorn and P. Bandaru, "Nanostructured thermoelectrics," Mater. Sci. Eng. R Rep. **67**, 19 (2010).
[4]A. Svilans, M. Leijnse, and H. Linke, "Experiments on the thermoelectric properties of quantum dots," C. R. Phys. **17**, 1096 (2016).
[5]P. Reddy, S.-Y. Jang, R. A. Segalman, and A. Majumdar, "Thermoelectricity in molecular junctions," Science **315**(5818), 1568–1571 (2007).
[6]Y. Dubi and M. Di Ventra, "Colloquium: Heat flow and thermoelectricity in atomic and molecular junctions," Rev. Mod. Phys. **83**, 131 (2011).
[7]H. Hammar, J. D. Vasquez Jaramillo, and J. Fransson, "Spin-dependent heat signatures of single-molecule spin dynamics," Phys. Rev. B **99**, 115416 (2019).
[8]G. Gadea, A. Morata, and A. Tarancon, "Semiconductor nanowires for thermoelectric generation," Semicond. Semimet. **98**, 321 (2018).
[9]L. Musland and E. Flage-Larsen, "Thermoelectric transport calculations using the Landauer approach, ballistic quantum transport simulations, and the Buttiker approximation," Comput. Mater. Sci. **132**, 146 (2017).
[10]L. Musland and E. Flage-Larsen, "Thermoelectric effect in superlattices; applicability of coherent and incoherent transport models," Comput. Mater. Sci. **153**, 88 (2018).
[11]D. Dragoman and M. Dragoman, "Giant thermoelectric effect in graphene," Appl. Phys. Lett. **91**, 203116 (2007).
[12]Y. Ouyang and J. Guo, "A theoretical study on thermoelectric properties of graphene nanoribbons," Appl. Phys. Lett. **94**, 263107 (2009).
[13]H. Zheng, H. J. Liu, X. J. Tan, H. Y. Lv, L. Pan, J. Shi, and X. F. Tang, "Enhanced thermoelectric performance of graphene nanoribbons," Appl. Phys. Lett. **100**(9), 093104 (2012).
[14]C. Pan, Z. Xie, L. Tang, and K. Chen, "Ballistic thermoelectric properties in graphene-nanoribbon-based heterojunctions," Appl. Phys. Lett. **101**, 103115 (2012).
[15]Z.-X. Xie, L.-M. Tang, C.-N. Pan, K.-M. Li, K.-Q. Chen, and W. Duan, "Enhancement of thermoelectric properties in graphene nanoribbons modulated with stub structures," Appl. Phys. Lett. **100**(7), 073105 (2012).
[16]H. Sevincli, C. Sevik, T. Cagin, and G. Cuniberti, "A bottom-up route to enhance thermoelectric figures of merit in graphene nanoribbons," Sci. Rep. **3**, 1228 (2013).
[17]B. Zhou, B. Zhou, Y. Zeng, G. Zhou, and T. Ouyang, "Seebeck effects in a graphene nanoribbon coupled to two ferromagnetic leads," J. Appl. Phys. **115**, 114305 (2014).
[18]C. Pan, Z. Xie, and K. Chen, in *Nanoscale Thermoelectrics*, edited by X. Wang and Z. M. Wang (Springer, 2014), Chap. 13, p. 393.
[19]M. I. Alomar and D. Sánchez, "Thermoelectric effects in graphene with local spin-orbit interaction," Phys. Rev. B **89**, 115422 (2014).
[20]P. Dollfus, V. H. Nguyen, and J. Saint-Martin, "Thermoelectric effects in graphene nanostructures," J. Phys. Condens. Matter **27**, 133204 (2015).
[21]V. Tran, J. Saint-Martin, P. Dollfus, and S. Volz, "Optimizing the thermoelectric performance of graphene nano-ribbons without degrading the electronic properties," Sci. Rep. **7**, 2313 (2017).
[22]P. Zolotavin, C. Evans, and D. Natelson, "Photothermoelectric effects and large photovoltages in plasmonic Au nanowires with nanogaps," J. Phys. Chem. Lett. **8**(8), 1739–1744 (2017).

© Author(s) 2019

[23]T. A. Amollo, G. T. Mola, M. S. K. Kirui, and V. O. Nyamori, "Graphene for thermoelectric applications: Prospects and challenges," Crit. Rev. Solid State **43**, 133 (2018).
[24]A. Harzheim, J. Spiece, C. Evangeli, E. McCann, V. Falko, Y. Sheng, J. H. Warner, G. Andrew, D. Briggs, J. A. Mol, P. Gehring, and O. V. Kolosov, "Geometrically enhanced thermoelectric effects in graphene nanoconstrictions," Nano Lett. **18**(12), 7719–7725 (2018).
[25]A. Sisman and I. Muller, "The Casimir-like size effects in ideal gases," Phys. Lett. A **320**, 360 (2004).
[26]W. Nie and J. He, "Performance analysis of a thermosize micro/nano heat engine," Phys. Lett. A **372**, 1168 (2008).
[27]W. Nie, J. He, and X. He, "A micro-/nanothermosize refrigerator and its performance analysis," J. Appl. Phys. **103**, 114909 (2008).
[28]T. Lin, G. Su, C. Ou, B. Lin, A. Le Méhauté, Q. A. Wang, and J. Chen, "Thermosize effects in confined quantum gas systems," Mod. Phys. Lett. B **24**(15), 1727–1737 (2010).
[29]G. Babac and A. Sisman, "Thermodynamic cycles based on classical thermosize effects," J. Comput. Theor. Nanosci. **8**, 1720 (2011).
[30]G. Babac and A. Sisman, "Classical thermosize effects in degenerate quantum gases," J. Comput. Theor. Nanosci. **8**, 2331 (2011).
[31]G. Su, L. Chen, T. Lin, and J. Chen, "Thermosize effects of ideal Fermi gases confined in micro/nano-scale tubes," J. Low Temp. Phys. **163**, 275 (2011).
[32]H. Wang, G. Wu, and X. Chen, "Thermosize effects and thermodynamic analysis of a macro/nano scaled refrigerator cycle," J. Appl. Phys. **111**, 024312 (2012).
[33]H. Wang and G. Wu, "Thermosize effects and irreversibility on the performance of a macro/nano scaled refrigeration cycle," J. Appl. Phys. **112**, 084325 (2012).
[34]A. Sisman and G. Babac, "Quantum size effects on classical thermosize effects," J. Continuum Mech. Therm. **24**, 339 (2012).
[35]H. Wang and G. Wu, "Ecological optimization for generalized irreversible macro/nano thermosize engine," J. Appl. Phys. **113**, 054309 (2013).
[36]H. Wang, G. Wu, X. Chen, and D. Chen, "Performance analysis and parametric optimum criteria of an irreversible macro/nano thermosize engine," J. Continuum Mech. Thermo. **25**, 43 (2013).
[37]G. Babac and J. M. Reese, "Molecular dynamics simulation of classical thermosize effects," Nanosci. Microsc. Therm. **18**, 39 (2014).
[38]S. Karabetoglu and A. Sisman, "Thermosize potentials in semiconductors," Phys. Lett. A **381**, 2704 (2017).
[39]W. Nie, K. Lu, A. Chen, J. He, and Y. Lan, "Performance optimization of single and two-stage micro/nano-scaled heat pumps with internal and external irreversibilities," Appl. Energy **232**, 695 (2018).
[40]M. Senay and S. Kibaroglu, "Thermosize effects in a q-deformed fermion gas model," Mod. Phys. Lett. B **32**, 1850230 (2018).
[41]C. W. J. Beenakker and H. van Houten, "Quantum transport in semiconductor nanostructures," Solid State Phys. **44**, 1 (1991).
[42]D. Gunlycke, H. M. Lawler, and C. T. White, "Room-temperature ballistic transport in narrow graphene strips," Phys. Rev. B **75**, 085418 (2007).
[43]J. Baringhaus, M. Ruan, F. Edler, A. Tejeda, M. Sicot, A. Taleb-Ibrahimi, A.-P. Li, Z. Jiang, E. H. Conrad, C. Berger, C. Tegenkamp, and W. A. de Heer, "Exceptional ballistic transport in epitaxial graphene nanoribbons," Nature **506**, 349 (2014).
[44]A. Celis, M. N. Nair, A. Taleb-Ibrahimi, E. H. Conrad, C. Berger, W. A. de Heer, and A. Tejeda, "Graphene nanoribbons: Fabrication, properties and devices," J. Phys. D Appl. Phys. **49**(14), 143001 (2016).
[45]S. Das Sarma, S. Adam, E. H. Hwang, and E. Rossi, "Electronic transport in two-dimensional graphene," Rev. Mod. Phys. **83**, 407–470 (2011).
[46]S.-F. Shi, X. Xu, D. C. Ralph, and P. L. McEuen, "Plasmon resonance in individual nanogap electrodes studied using graphene nanoconstrictions as photodetectors," Nano Lett. **11**(4), 1814–1818 (2011).
[47]L. Rosales and J. W. Gonzalez, "Transport properties of two finite armchair graphene nanoribbons," Nanoscale Res. Lett. **8**, 1 (2013).
[48]C. W. Groth, M. Wimmer, A. R. Akhmerov, and X. Waintal, "Kwant: A software package for quantum transport," New J. Phys. **16**, 063065 (2014).
[49]S. Reich, J. Maultzsch, C. Thomsen, and P. Ordejón, "Tight-binding description of graphene," Phys. Rev. B **66**, 035412 (2002).
[50]Y. Hancock, A. Uppstu, K. Saloriutta, A. Harju, and M. J. Puska, "Generalized tight-binding transport model for graphene nanoribbon-based systems," Phys. Rev. B **81**, 245402 (2010).
[51]S. Datta, *Electronic Transport in Mesoscopic Systems* (Cambridge University Press, 1995).
[52]W. X. Zhou and K. Q. Chen, "Enhancement of thermoelectric performance in beta-graphyne nanoribbons by suppressing phononic thermal conductance," Carbon **85**, 24 (2015).
[53]X. K. Chen, Z. X. Xie, W. X. Zhou, L. M. Tang, and K. Q. Chen, "Phonon wave interference in graphene and boron nitride superlattice," Appl. Phys. Lett. **109**, 023101 (2016).
[54]X. K. Chen, J. Liu, Z. X. Xie, Y. Zhang, Y. X. Deng, and K. Q. Chen, "A local resonance mechanism for thermal rectification in pristine/branched graphene nanoribbon junctions," Appl. Phys. Lett. **113**, 121906 (2018).
[55]D. Liu *et al.*, "Raman enhancement on ultra-clean graphene quantum dots produced by quasi-equilibrium plasma-enhanced chemical vapor deposition," Nat. Commun. **9**(1), 193 (2018).
[56]M. Jung *et al.*, "GHz nanomechanical resonator in an ultraclean suspended graphene p–n junction," Nanoscale **11**, 4355–4361 (2019).

© Author(s) 2019